

We are IntechOpen, the world's leading publisher of Open Access books Built by scientists, for scientists

6,900

Open access books available

186,000

International authors and editors

200M

Downloads

Our authors are among the

154

Countries delivered to

TOP 1%

most cited scientists

12.2%

Contributors from top 500 universities



WEB OF SCIENCE™

Selection of our books indexed in the Book Citation Index
in Web of Science™ Core Collection (BKCI)

Interested in publishing with us?
Contact book.department@intechopen.com

Numbers displayed above are based on latest data collected.
For more information visit www.intechopen.com



Numerical Solutions for Structural Relaxation of Amorphous Alloys Studied by Activation Energy Spectrum Model

Kazu-masa Yamada

Additional information is available at the end of the chapter

<http://dx.doi.org/10.5772/53723>

1. Introduction

What is the physical process which is producing the general characteristic of glass? It is said that the transformation of the liquid-system to glass one is a final theme in physics through into the twenty-first century. Furthermore, the development of amorphous-material devices and specimen modification methods is closely related with the obviousness of high thermal stability and stability of relaxation.

The aim of this research is to clarify numerical solutions for nano-structure relaxation processes focusing on the activation energy in transition metal (ie Cu, Fe) based amorphous alloys. Activation energy for structural relaxation process in a metal type amorphous ternary and quaternary alloys, with cross sections of typically 0.03 mm x 2.0 mm, prepared by chill-block melt spinning has been investigated by Differential Scanning Calorimetry (DSC) with a cyclically heating technique [1,2,3]. Activation energies for structural relaxation with a spatial quantity in amorphous materials have been discussed by use of a total relaxed ratio function that depends on annealing temperature and time. In the present work in amorphous ternary and quaternary alloys, the distributions for the Activation Energy Spectrum (AES) with derivative-type relaxed ratio function were observed. Another result has been also established that the "reversible" AES model energy distribution though the cyclically nano-structural relaxations were in good agreement with the presented experimental results of transition metal based amorphous alloys.

There has been recently considerable that the glassy alloys are representative of the bulk formed ultra-fine structure [1]. Particularly Cu has been shown to be good base element for bulk glass-forming alloy with fully glassy sections recently by use of die injection casting [2,3]. Binary Cu - (Zr or Hf) alloys have been found to form an amorphous phase over a

wide composition range. However, addition of Ti in both these binary systems greatly increased the glass forming ability (GFA), with the critical diameter for fully amorphous rods being at least 4 mm for $\text{Cu}_{60}\text{Zr}_{30}\text{Ti}_{10}$, $\text{Cu}_{60}\text{Hf}_{20}\text{Ti}_{20}$ and $\text{Cu}_{55}\text{Hf}_{25}\text{Ti}_{20}$ [2,3]. Meanwhile the understanding of the structural relaxation process is essential in the development of stability for amorphous alloys, as well as in establishing stable working temperature to avoid the degradation of strength. Therefore, high thermal stability of quasi-stable amorphous materials for Cu based alloys. The atomic mechanism of diffusion in amorphous alloys is still poorly understood as compared to that in crystalline alloys. However, measurements of diffusivity in amorphous alloys have been limited so far because of the experimental difficulties of measuring the very small diffusion coefficients, usually less than $10^{-17} \text{ m}^2\text{s}^{-1}$, which are typical of amorphous alloys below their crystallization temperatures [4,5].

In the present work, using Differential Scanning Calorimetry (DSC) thermal analysis has been made to determine the activation processes [6,7,8], and to evaluate whether it represents the thermodynamically stable form of CuHfTi and CuHfTi-B glass-forming amorphous alloys.

2. Experimental procedure

Cu-based alloy ingots of composition $\text{Cu}_{60}\text{Hf}_{20}\text{Ti}_{20}$, $(\text{Cu}_{60}\text{Hf}_{22}\text{Ti}_{18})_{0.99}\text{B}_1$ and $(\text{Cu}_{60}\text{Hf}_{22}\text{Ti}_{18})_{0.97}\text{B}_3$ were prepared by arc-melting mixtures in an argon gas atmosphere purified with a Ti getter. The alloy compositions represent the nominal values but the weight losses in melting were negligible. The alloy ingots were inverted on the hearth and re-melted several times, to ensure compositional homogeneity. Ribbon samples of each alloy, with cross sections of typically $0.03 \text{ mm} * 2.0 \text{ mm}$, were produced by chill-block melt spinning in a sealed inactive gas atmosphere. The amorphous state of the specimen of the ribbon samples was confirmed by X-ray diffraction.

The endothermic/exothermic heats for relaxation process were measured by differential scanning calorimetry (DSC) of DSC3100s of MacScience Co., Ltd (Bruker Japan Co., Ltd.) at a constant heating rate of 1.00 K/s. And the ordered specimens were prepared by annealing used in the electric furnace of the DSC. Pre-annealing and following long-time main annealing by a DSC furnace are at a 700 K for 1800 s and at a 580 K for 6000 s, respectively. The maximum temperature of 700 K is enough to suppress the crystallization and to measure optimistically the structural relaxation for these three kinds of specimen [9].

2.1. Theory with DSC annealing process

Due to insufficient data of thermal stability of amorphous alloys, the following points are left as future problems. Even bulk glass-forming alloy, also amorphous alloys is a non-equilibrium state. The certain overall atoms in an amorphous alloy are in non-stable state rather than in the stable crystalline state. Therefore, not only crystallization over a certain wide temperature range but also re-arrangement of atoms occurs. The structural relaxation process is one of the essential phenomena in some non-equilibrium materials. Thereby, to

study the structural relaxation is important to investigate the constitutional property of the amorphous alloys. Furthermore, the structural relaxation is closely connected with the stability of specific examples related to the bulk glass-forming amorphous alloy. It is also necessary to know this property from a viewpoint of the application development.

Consider the population of an assembly of reaction centre for structural relaxation, that is to say isolated double wells potential model (or so called Two Level System, TLS) as shown in Fig. 1[9]. A relaxation centre which is isolated and in a particular structural configuration, permits an atom to be either in a higher energy position at state 0 or in a lower energy position at state 1 in Fig. 1. The axis of abscissas is the configuration variable for relaxation processes, and the position $1/2$ on the axis in Fig.1 is the saddle point for the energy wall between the position 0 and 1.

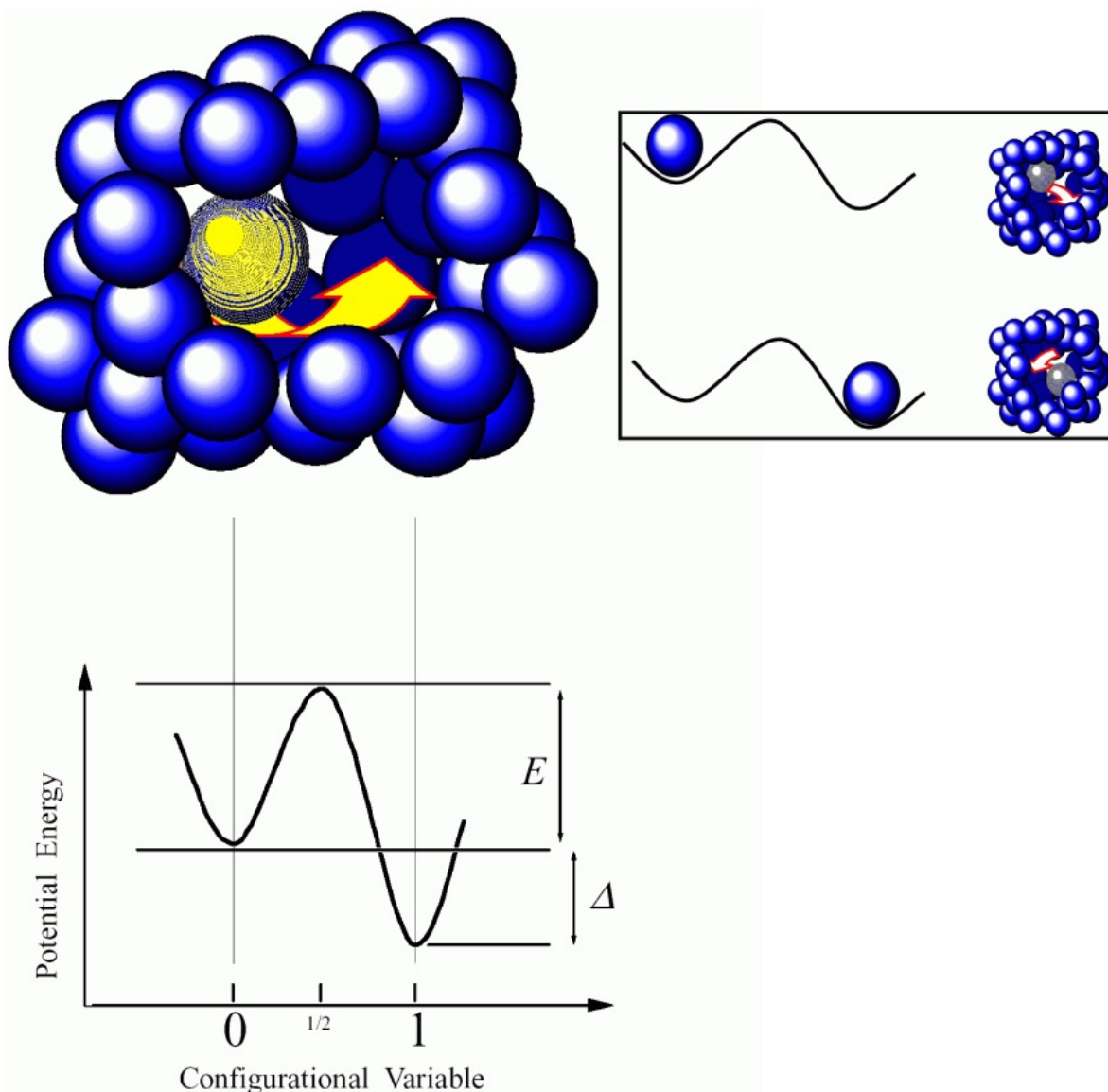


Figure 1. Schematic illustrations of relaxation centre and energy levels for the corresponding two level system

On the population of an assembly of this model, activation energy spectrum (AES) in structural relaxation processes, J. A. Leake, J. E. Evetts and M. R. J. Gibbs [10,11] describe the phenomena of physical available and variable property with good agreement between the theory and the experimentation. The theory assumes exponent factor nearly equal one-dimension for chemical reaction kinetics of Johnson-Mehl-Avrami (JMA) equation.

Therefore, the theoretical model for the relaxation process in amorphous materials on the basis of a spectrum of available processes with a distribution of activation energy was proposed. In their model, the total change in the measured property, ΔP is given by

$$\Delta P = \int_0^E p(E)dE \quad (1)$$

In the range of activation energy E to $E+dE$ during the structural relaxation process, the total available property $p_0(E)$ changes such as

$$p(E)dE = p_0(E) \left[1 - \exp \left\{ -\nu_0 t \exp \left(-\frac{E}{kT} \right) \right\} \right] dE \quad (2)$$

where ν_0 is an order of the Debye frequency ($\nu_0 \cong 10^{12}$ Hz) . Primak [12] rewrites Eq. (2) as

$$p(E) = p_0(E) \theta(E, T, t), \quad (3)$$

where $\theta(E, T, t)$ is defined as the characteristic annealing function. Thus, the function of $\theta(E, T, t)$ is a measure of the proportion of available processes at the energy E . Proportion as $\theta(E, T, t)$ has contributed to the relaxation property after the time t at the annealing temperature T . The form of $\theta(E, T, t)$ is given in Fig. 2 (a) and (b) .

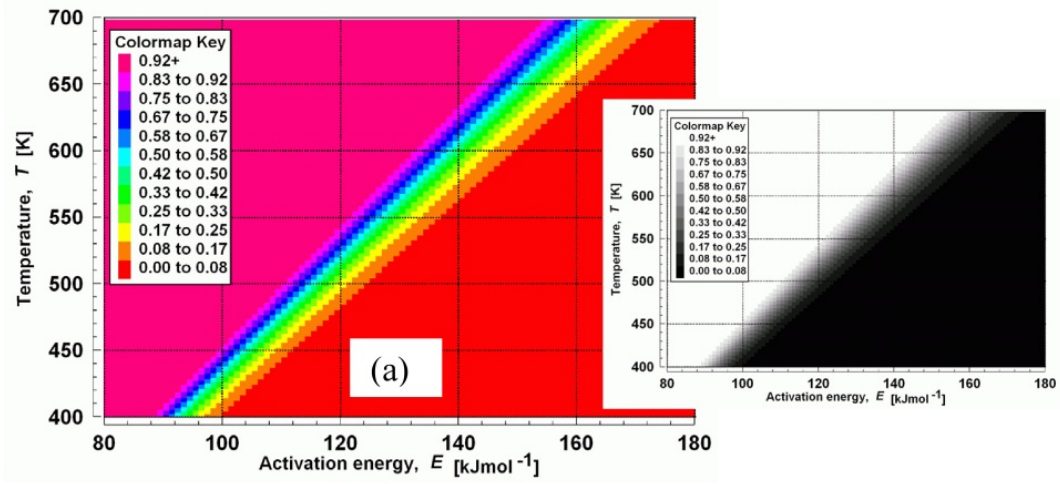
In the another paper [9], in a process for most simplifying assumption, the function $\theta(E, T, t)$ can be replaced by step function at an energy $E_0(T, t)$ as

$$E_0 = kT \ln(\nu_0 t) \quad (4)$$

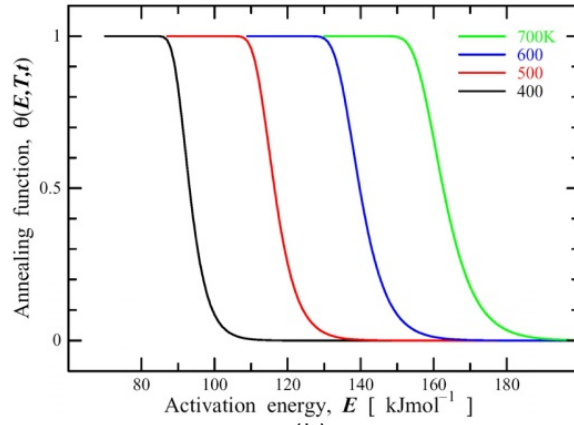
These E_0 forms are given in Fig. 2 (c, d, e, f, g, h, i), then E_0 changes from 0 to 1 over one-step meanwhile $\theta(E)$ changes over a narrow range of E and T . If in the simplified calculations, the E_0 should have been applied. On the other hand, in the present work for calculation using specific 1st derivative-type relaxation ratio, as follows.

$$\frac{d\theta(E, T, t)}{dE} = \left\{ \nu_0 t \exp \left(-\frac{E}{kT} \right) \right\} \left(-\frac{E}{kT} \right) \exp \left\{ -\nu_0 t \exp \left(-\frac{E}{kT} \right) \right\} \quad (5)$$

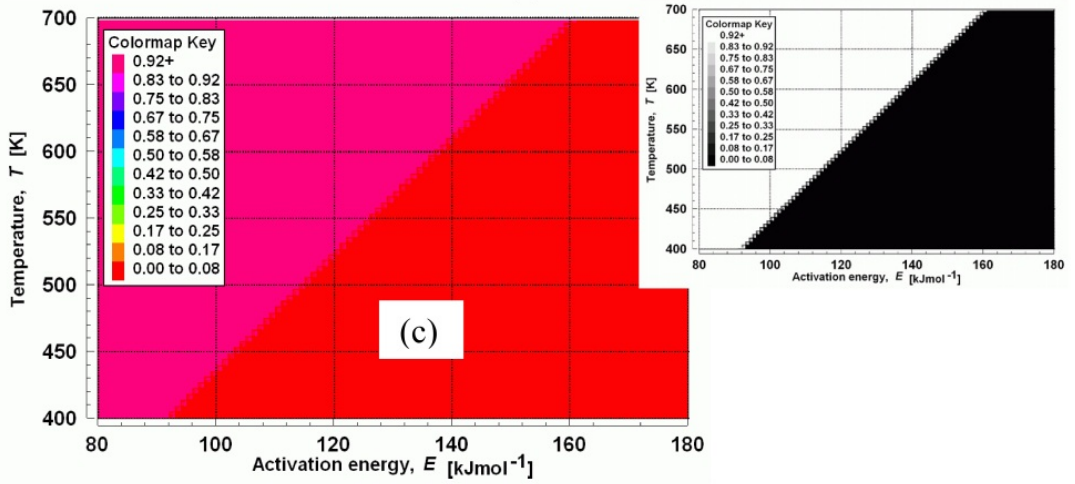
The (5) function is shown in Fig 3 (a), on the contrary the derivative of $E_0(T)$ is shown in Fig 3 (b) . So it should be preferred replacement with a better approximation using the function (5). By using simple area summation method, furthermore the normalization for the linear function of $S=0.234 T+0.244$ in this case as shown in Fig 4 would be applied, we can estimate the actual activation energy spectra distributions using the method of Fig 5. It is so called normalized 1st derivative - type relaxation ratio function in our organized work.



(a)



(b)



(c)

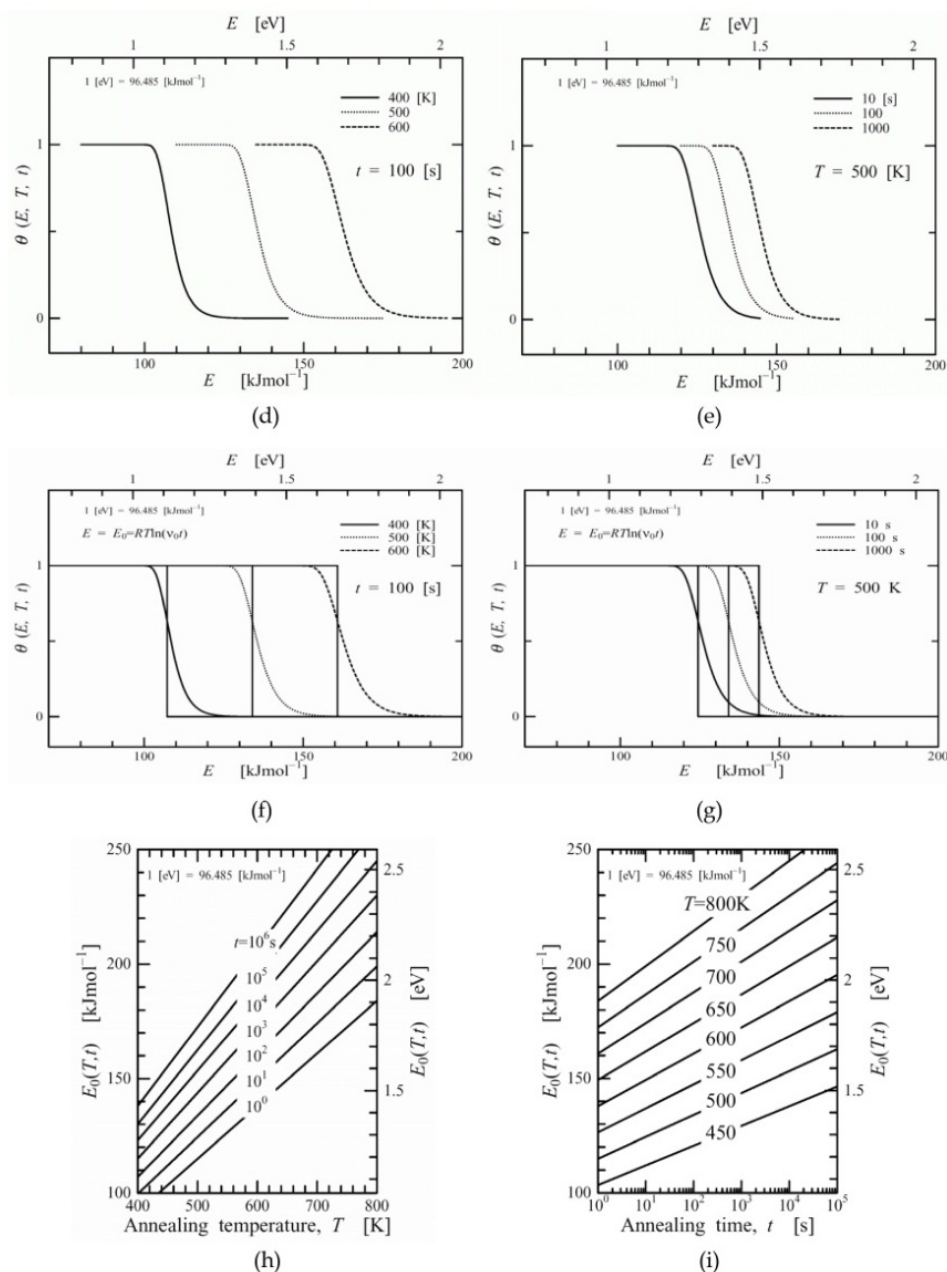


Figure 2. (a). Dependence of the characteristic annealing function $\theta(E, T, t=1s)$ on the activation energy E and the temperature T [9,10]. Fig. 2(a) is used of $\theta(E, T, t=1s)$ (b). Dependence of the characteristic annealing function $\theta(E, T, t=1s)$ on the activation energy E and the temperature T [9,10]. Fig. 2(b) is used of $\theta(E, T, t=1s)$ (c). Dependence of the characteristic annealing function $\theta(E, T, t=1s)$ on the activation energy E and the temperature T [9,10]. Fig. 2(c) is used of $E_0(T, t=1s)$. Right hand and left hand of charts are the same figure. Additionally right one is shown in grey scale for visible-contrasty (d,e,f,g). Dependence of the characteristic annealing function $\theta(E, T, t)$ and step function of threshold $E_0(T, t)$ on the horizontal axis of the activation energy E [9,10]. Fig. 2(d) at the upper left is used of $\theta(E, T, t=100s)$. Fig. 2(e) at the upper right is used of $\theta(E, T=500K, t)$. Fig. 2(f) at the lower left is used with step functions superposed on $\theta(E, T, t=100s)$. Fig. 2(g) at the lower right is used with step functions superposed on $\theta(E, T=500K, t)$ (h, i). Dependence of the simplifying assumption of characteristic annealing function, activation energy $E_0(T, t)$ vs the annealing time t and the isothermal annealing temperature T [9,10]. Fig. 2(h) at the left is used of $E_0(T, t=1, 10, 10^2, 10^3, 10^4, 10^5$ and 10^6 s). Fig. 2(i) at the right is used of $E_0(T=450, 500, 550, 600, 650, 700, 750$ and $800K)$

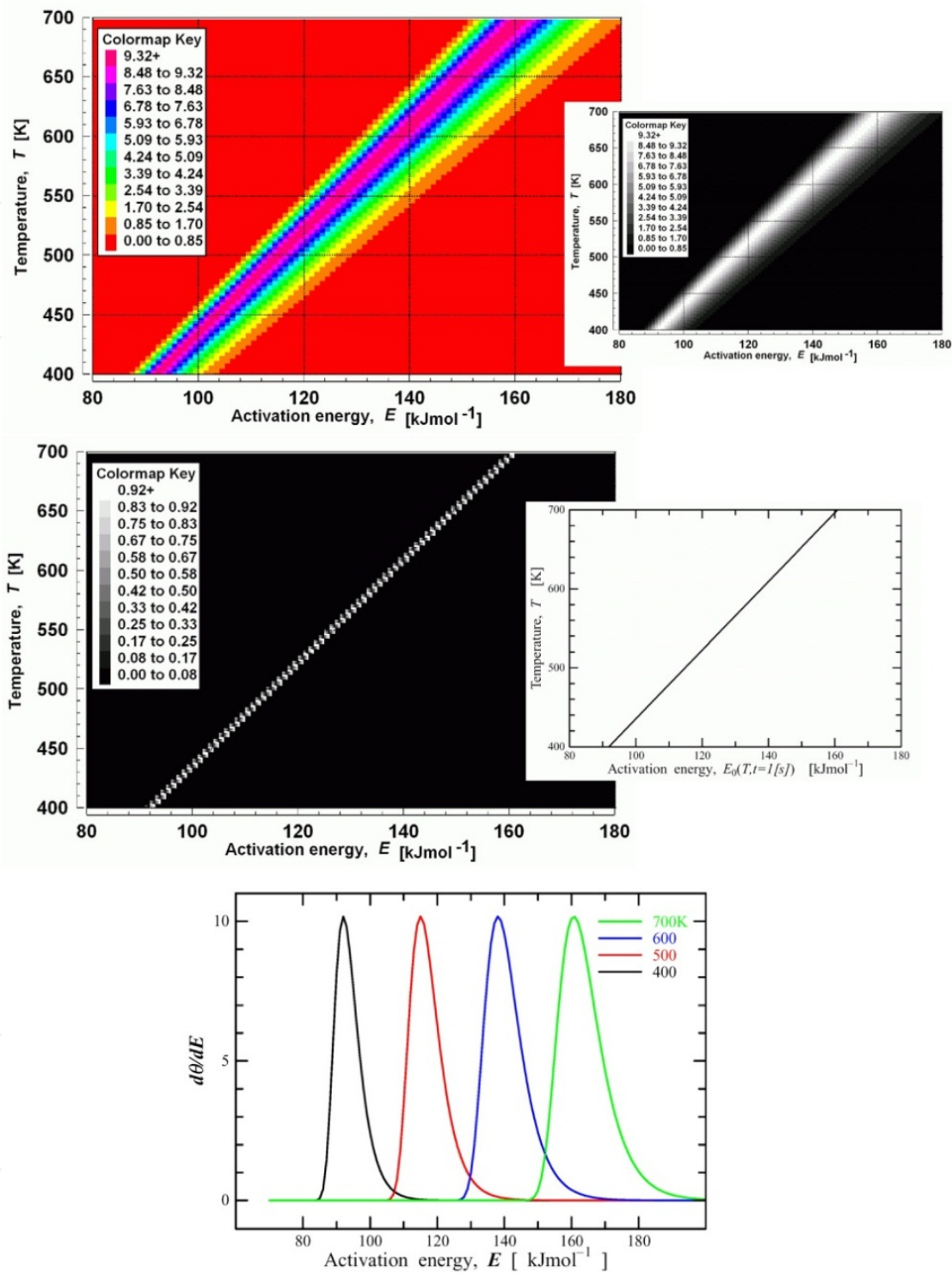


Figure 3. (a). Dependence of the 1st derivation of θ ($E, T, t=1$ s) on the activation energy E and the temperature T . Fig. 3 (a) Derivative type $\theta(E, T, t=1$ s). Right hand and left hand of charts are the same figure. Additionally right one is shown in grey scale for visible-contrast (b). Dependence of the 1st derivation of θ ($E, T, t=1$ s) on the activation energy E and the temperature T . Fig. 3 (b) Approximation type $E_0(T, t=1$ s). Right hand and left hand of charts are the same figure. Additionally right one is for visible-contrast (c). Dependence of the 1st derivation of θ ($E, T=400, 500, 600$ and $700\text{K}, t=1$ s) on the activation energy E .

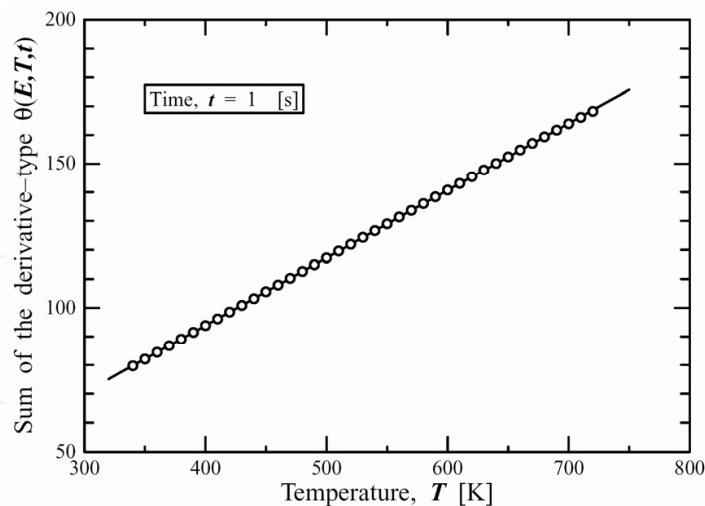


Figure 4. Dependence of the summation S of 1st derivative type $\theta(E, T, t=1s)$ on the temperature T . Plots can be replaced by linear function with a good approximation in $S = 0.234 T + 0.244$

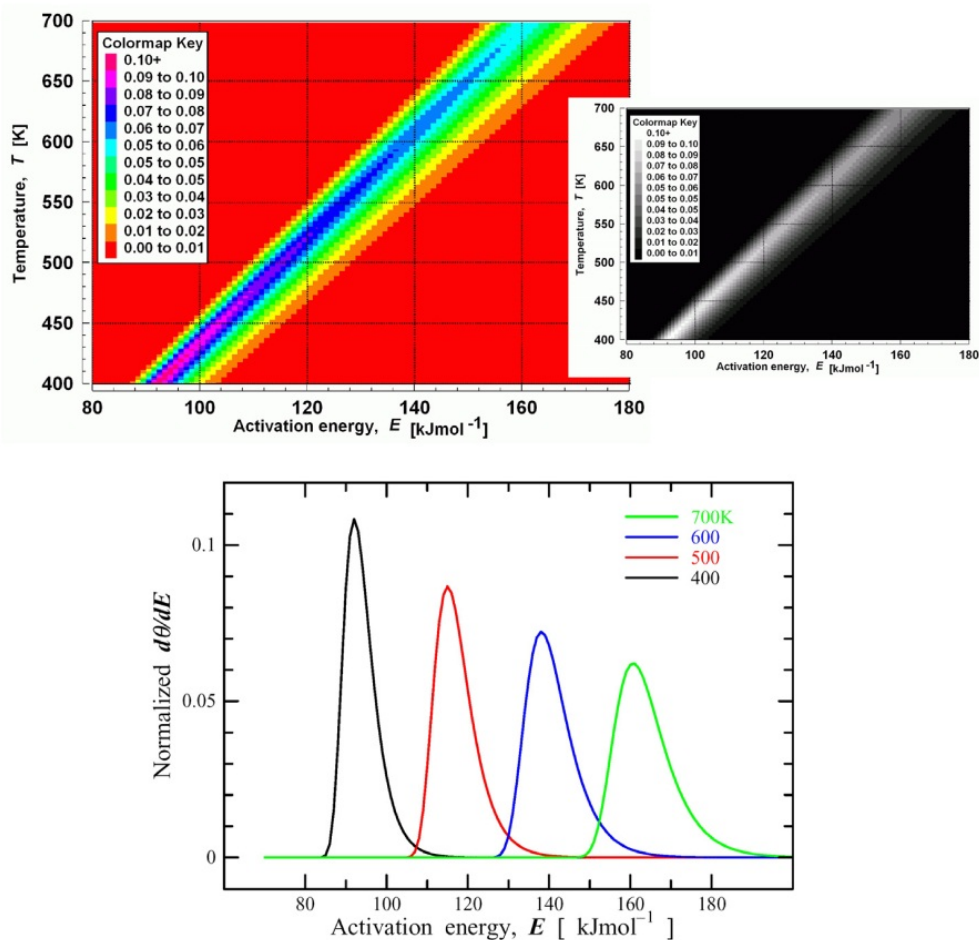


Figure 5. (a). Divided by the $S = 0.234 T + 0.244$ of Fig 4, dependence of the normalized 1st derivative-type relaxation ratio function of $\theta(E, T, t=1s)$ on the activation energy E and the temperature T . Right hand and left hand of charts are the same figure. Additionally right one is shown in grey scale for visible-contrasty (b). Divided by the $S = 0.234 T + 0.244$ of Fig 4, dependence of the normalized 1st derivative-type relaxation ratio function of $\theta(E, T=400, 500, 600$ and $700K, t=1 s)$ on the activation energy E

2.2. Experimental processes with DSC annealing

In the previous paper [9], we discussed at first the AES applied on the Cu-Hf-Ti system, because of the following reasons.

In Table 1 [2] the glass forming ability (GFA) related to the T_{rg} ($=T_g / T_L$) was observed that addition of Ti in Cu-Hf binary systems greatly increased. In this table, they were shown with the critical diameter d_C for fully amorphous rods being at least 3 mm for $Cu_{60}Hf_{22.5}Ti_{17.5}$, $Cu_{60}Hf_{20}Ti_{20}$ and $Cu_{60}Hf_{17.5}Ti_{22.5}$.

Composition	d_C	T_g (K)	T_X (K)	T_L (K)	T_{rg} ($=T_g / T_L$)
$Cu_{60}Hf_{35}Ti_5$	Ribbon	775	828	1333	0.58
$Cu_{60}Hf_{30}Ti_{10}$	Ribbon	751	806	1263	0.59
$Cu_{60}Hf_{25}Ti_{15}$	Ribbon	748	788	1240	0.60
$Cu_{60}Hf_{22.5}Ti_{17.5}$	4mm	745	780	1234	0.60
$Cu_{60}Hf_{20}Ti_{20}$	4mm	740	767	1211	0.61
$Cu_{60}Hf_{17.5}Ti_{22.5}$	3mm	732	755	1229	0.59
$Cu_{60}Hf_{15}Ti_{25}$	Ribbon	722	745	1223	0.59
$Cu_{60}Hf_{10}Ti_{30}$	Ribbon	700	726	1233	0.56
$Cu_{60}Hf_5Ti_{35}$	Ribbon	690	712	1223	0.56

Table 1. Glass forming section thickness and thermal property for $Cu_{60}Hf_{40-X}Ti_X$ (X =from 5 to 35) alloy series [2]

After all, the aim of this research is also to clarify a quantitative evaluation in the structure relaxation processes focusing on the activation energy in $Cu_{60}Hf_{20}Ti_{20}$ based amorphous alloys with high GFA series.

Pre-annealing and main-annealing conditions were completely similar the way as Ref. 9. After that it will be noted that an atom to be in a higher energy position at stage 0 in Fig. 1, endothermic heat occurs at 1st run in the measurement scanning #1 even at 1st run in #2, that is to say the reversible relaxation processes, and the 1st minus 2nd run indicates the endothermic value (the 2nd minus 1st run indicates the exothermic value) that could be calculate the AES distributions that means an atom to be in a higher energy position at stage 0 in Fig. 1.

The liquidus temperature T_L has its minimum value for the 20at%Ti alloy in Table 1, probably corresponding to a ternary eutectic system, it is because only this composition has single melting peak in the DTA trace [2]. Thus this is a dominating factor in determining that T_{rg} has its maximum value at this composition clearly. The atomic diameter of Ti (0.289nm) is intermediate between those of Cu (0.256nm) and Hf (0.315nm) and, evidently, equal proportions of Hf and Ti result in maximum stabilization of the densely packed liquid structure [2] and normalized 1st derivative - type relaxation ratio function.

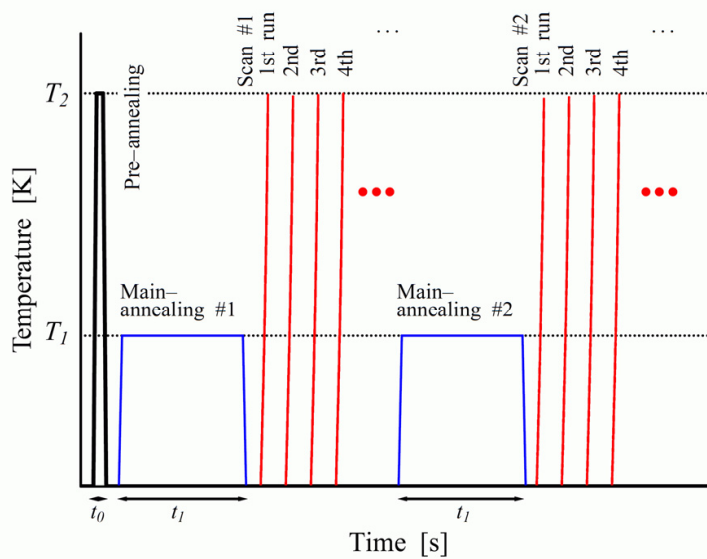


Figure 6. An example of annealing time and temperature history by use in fully electric furnace of the DSC. Specimens were prepared by annealing used in the DSC furnace, pre-annealing and following long-time main-annealing are at 700 K ($=T_2$) for 1800 s ($=t_0$) and recycled at a 580 K ($=T_1$) for 6000 s ($=t_1$), respectively. The maximum temperature of T_2 is enough to suppress the crystallization and to measure optimistically the structural relaxation following the continuous scan #1 1st run to n-th run. The "reversible" phenomena have been observed in the anneal process of scan #2 to scan #n as shown in Fig.7.

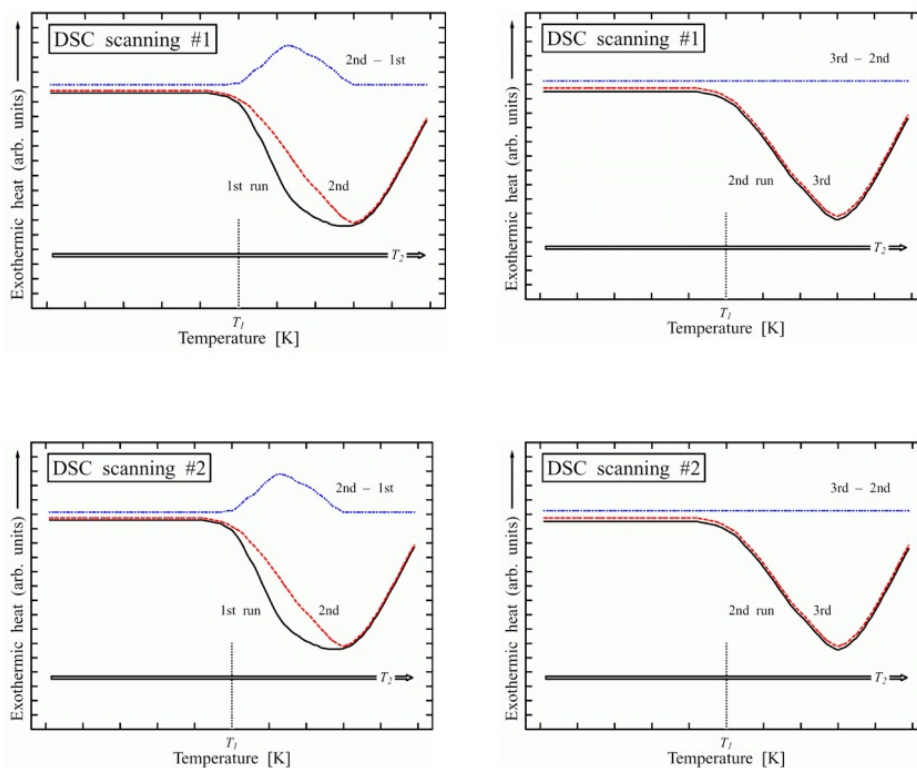


Figure 7. four-leaved schematic illustrations of reversible phenomena for DSC scanning #1 then #2, and included relaxation processes for scanning 1st run then 2nd run, on the other hand without relaxation processes for scanning 2nd run then 3rd run

3. Results through experimental procedure

In the presented work by use of the AES model, following above-mentioned, activation energies in structural relaxation processes have been determined of composition $\text{Cu}_{60}\text{Hf}_{20}\text{Ti}_{20}$ and related $(\text{Cu}_{60}\text{Hf}_{22}\text{Ti}_{18})_{0.99}\text{B}_1$ and $(\text{Cu}_{60}\text{Hf}_{22}\text{Ti}_{18})_{0.97}\text{B}_3$ amorphous alloys as shown in Fig. 8.

The maximum energies in AES have similar tendency among three kinds of alloy nearly at 160 kJmol^{-1} (1.66 eV). Between the three kinds of B for 3, 1 and 0 % alloys, in an energy region less than 160 kJmol^{-1} , AES of only B 3 % alloy is higher than that of B 1% and 0 %.

Meanwhile, in an energy region more than 160 kJmol^{-1} , AES of them are similar. This suggests that the diffusion path size for the diffusant of Ti that atomic radius is smallest in the metallic compositions and the packing density of the covalent bonding matrix between the boron and metal are dominant in the relaxation processes. Consequently activation energy for the structural relaxation process has been determined in the $\text{Cu}_{60}\text{Hf}_{20}\text{Ti}_{20}$ with having the highest bulk glass-forming ability in $\text{Cu}_{60}\text{Hf}_{40-X}\text{Ti}_X$ (X are from 5 to 35 %) alloy series as almost 160 kJmol^{-1} (1.66 eV) using the normalized derivative - type relaxed ratio function [9].

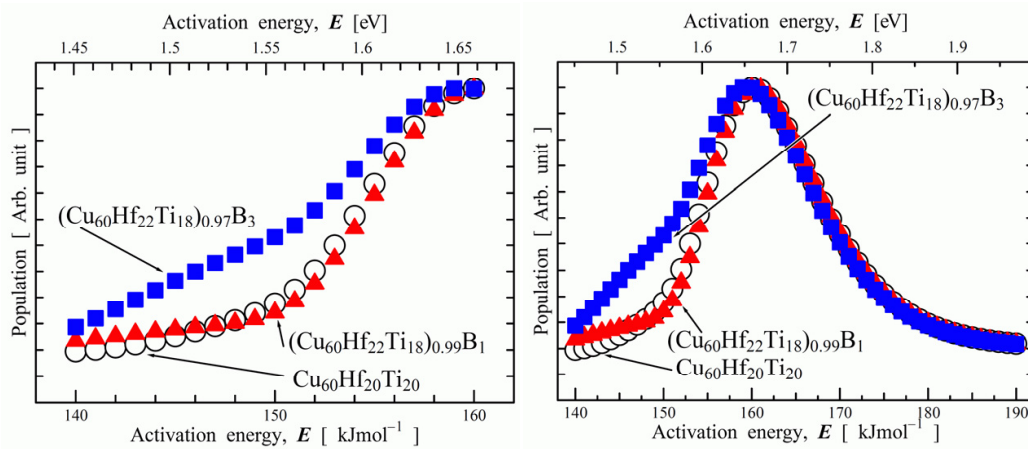


Figure 8. In the present work for calculation using specific normalized 1st derivative - type relaxation ratio function of $\theta(E, T, t=1s)$, activation energy spectrum distributed in $\text{Cu}_{60}\text{Hf}_{20}\text{Ti}_{20}$, $(\text{Cu}_{60}\text{Hf}_{22}\text{Ti}_{18})_{0.99}\text{B}_1$ and $(\text{Cu}_{60}\text{Hf}_{22}\text{Ti}_{18})_{0.97}\text{B}_3$

4. Calculation technique

In the Fig. 7., four-leaved schematic illustrations show on the DSC scanning #1, #2, we could evaluate the value included relaxation processes for scanning 1st run then 2nd run, on the other hand we could estimate the value included not relaxation processes for scanning 2nd run then 3rd run that are almost without relaxation. So solving the value should be calculated by DSC exothermic heats of 2nd run minus 1st run. So it is very important to calculate the differences between 2nd and 1st run. But also it is difficult to calculated form the DSC exothermic heats of 2nd run minus 1st run because of the temperature scanning step problem. This section describes the way of calculation how to get the differences (distinction) data.

In the Fig. 9., if they were a typical numerical example for differential calculation with supplied as text-type file name, for example, TEST00.TXT of 1th DSC run and TEST01.TXT of 2nd one, it would be transformed from their differential calculation to result numerical data such as TEST04.TXT, to be free to use a program such as GP.EXE ver. 4.13 and DOSBox version 0.74. The 2-Dimension Graph Plotter GP.EXE version 4.13-PC/AT and Dos-emulator DOSBox version 0.74 for all kind of MS-windows OS (another DOSBox version exists for MAC OS probably) are both free software supported in English keyboard peripheral interface. Additionally information, the GP.EXE was built by Prof. Dr. K. Edamatsu(now at riec.tohoku.ac.jp) in 1980-99 year for design to plot scientific/engineering graphs using PCs. Prof. Edamatsu said in his GP's documentation "with GP.EXE, make smart graphs for your presentation and publication. Also, try GP's powerful data analysis capability such as general least-squares fitting, numerical differentiation and integration".

In around 2010 year, the GP.EXE with super high speed and powerful data analysis capability is born-again by use of high performance Dos-emulator DOSBox.

Presented process, to calculate the differential exo/endothemic heat supplied from DSC live scanning environmental with gas flow atmosphere. Overall, Relaxation processes for example has been tutorial as bellow description mainly using the freeware GP.EXE, further only using scanning data 1st run to 2nd run.

In the Fig. 10., for introduction to present calculation technique, typical complex 2-D tutorial graph samples are shown by using GP.EXE. A left chart is the typical Gaussian differentiation tutorial sample, 1st derivative and 2nd one and experimental data and calculation. A right chart is the typical Ahhrenius tutorial plot with inversed horizontal axis with logarithm vertical axis. If you were to use the GP.EXE, you should download from the site of www.vector.co.jp/soft/dos/business/se004831.html.

Then you could get the file of `gpat431.lzh`, you should make the directory for set the GP.EXE environments. It should be save and destination to (recommended): `C:/prog/gp/gp.exe`, `C:/prog/gp/INIT.GPR`, `C:/prog/gp/DOC`, `C:/prog/gp/ DRIVERS`, etc.

Note: GP.EXE system is so called legacy-DOS, overall generated user filename must be kept the name rule of 8 character letter filename and 3 character letter extensions around in the GP directory.

Addition you could get the file of `gpsmp420.lzh` of tutorial examples of GPR extension files, you could be easy to get the way the GP.EXE operating. As shown in Fig. 10., the tutorials exist in site of www.vector.co.jp/soft/dos/business/se010753.html.

In the Table 2. , Recommended Dos-emulator DOSBox version 0.74 configuration file descriptions are shown. You could edit (ie. MS-Win7) it in Program Menu, DOSBox options, editing the configuration, last lines for "autoexec" region. Addition, **keyb** command needs the user of Japanese JP106 keyboard peripheral interface only (addition the **keyb** program and keyboard-map should also be needed. The **keyb** system's useful information would be gathered in World Wide Web). Meanwhile for in English peripheral US101 user, the **keyb** command should be ignore. Furthermore the last **gp** command in table 2, it should not be

need to user for non-automatic start of GP. For normal user, it should be ignore the last one. Otherwise all users command the type key of **gp** on DOSBox command line , GP.EXE starts anytime.

```
[autoexec]
# Lines in this section will be run at
startup.
# You can put your MOUNT lines here.
@ECHO OFF
MOUNT c C:\
c:
```

Table 2. A sample of Dos-emulator DOSBox version 0.74 configuration file description (as shown in autoexec area only)

In the Fig. 11., GP.EXE column structure menu indicating live date column was shown. In the case, X, Y, YE of default column structure allow to use a delimiter also space and tabulator key. Live data should be minimum structure of X and Y with delimiter of space key. Meanwhile additional data column if include could be were specially galloped by use of “U” rule for GP column structure. The typical sample structure of live data is shown in Table 3a and 3b. Addition the 1st, 2nd and 3rd line were normally (default) galloped through a whole text-file for GP because of a purpose for a title and axis captions.

INIT.GPR and other GPR files would be able to modified by a text-type general-purpose editor, then directory file path, captions and so on in them could be also re-arranged and rapid setting for similar graph format preparations.

Note: GPR file always includes full-Path towards live data, but usually it is NOT often need to full-Path towards them but only Local-Path that means without non-Path description, then some of this full-Path should be deleted by use of a text-type general-purpose editor because of keeping the safety-connection between the live data and the GPR file.

In the Fig. 12., load file name menu indicates the live date formatted general-purpose text-style pursuant to table 3a,3b. As it was shown, 3 files (2 kinds of file) of TEST00.TXT, TEST01.TXT and TEST00.TXT are loaded in the live data tray in GP.EXE for 2 data differential calculations. The file #1 should be without differential calculations. The file #2 and #3 should be with differential calculation for #3 minus #2.

In the Fig. 13., load and save parameter’s file (GPR of extensions) menu indicates graph structure list organized whole graphic design. Especially GPR file is also plain text-type, so we could arrange them before/afterward by use of a text-type general-purpose editor anytime.

Note: GP.EXE system is so called legacy-DOS, overall generated user filename must be kept the name rule of 8 character letter filename and 3 character letter extensions around in the GP directory.

In the Fig. 14., a Interfile Calculation Parameters and style-menu displayed, red-mark of TEST01 (Src. file # 2) on left-y-axis and white-mark of TEST00 (Src. file # 1) on left-y-axis, meanwhile blue-mark of TEST00 minus TEST01 (Src. file #3 minus #2) on right-y-axis. The aim of this computation is to process the file #3 minus #2 based rule on column X date for Temperature region. Finally a result of the processed data has been shown as blue-mark beside on right-y-axis.

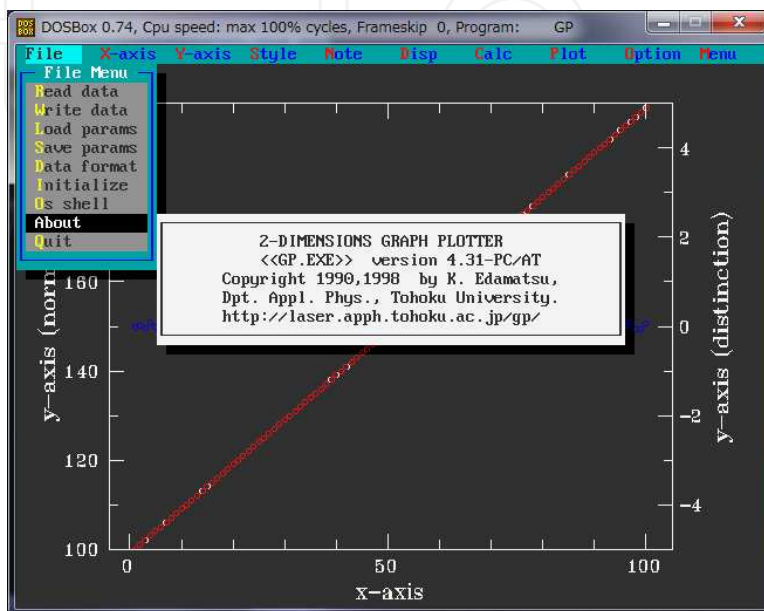


Figure 9. 2-Dimension Graph Plotter GP.EXE version 4.13-PC/AT and Dos-emulator DOSBox version 0.74 are both free software in English supported to calculate the differential exothermic heat data using DSC included relaxation processes for example, scanning 1st run to 2nd run.

GP.EXE: <http://www.vector.co.jp/soft/dos/business/se004831.html>

GP.EXE samples :<http://www.vector.co.jp/soft/dos/business/se010753.html>

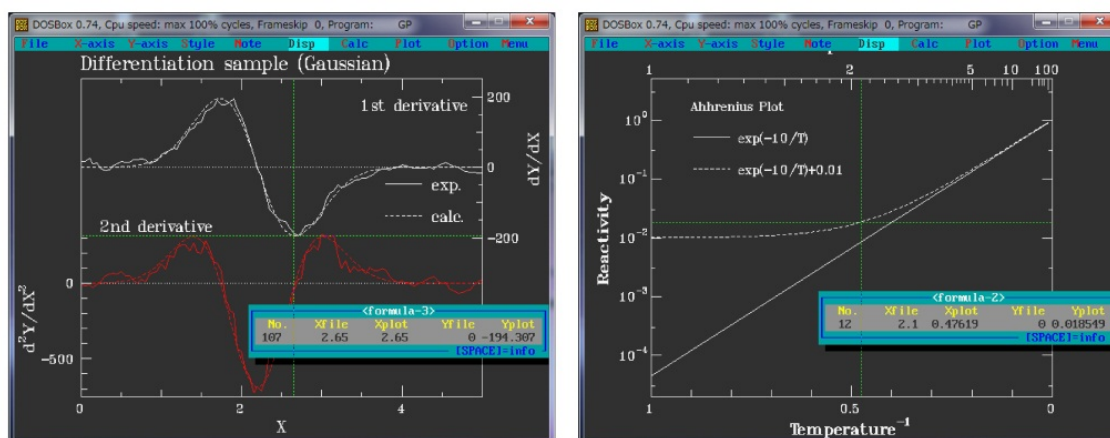


Figure 10. Typical samples of 2-Dimension Graph Plotter GP.EXE. A left chart is the typical Gaussian differentiation sample, 1st derivative and 2nd one and experimental data and calculation. A right chart is the typical Ahrens-type plot with inversed horizontal axis together with logarithm vertical axis. Green colour cross line indicator means the across point both live-data and translated-data.

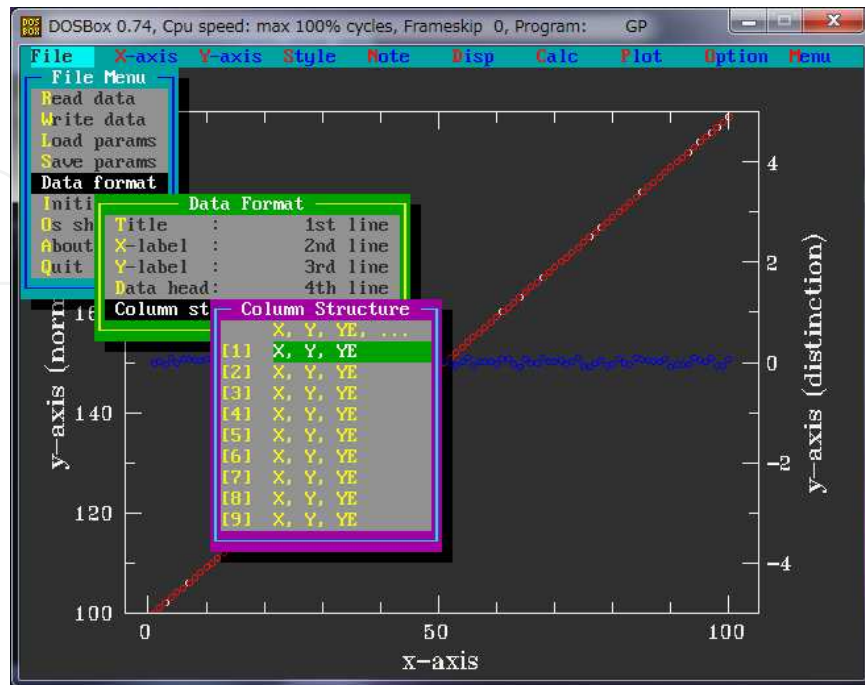


Figure 11. At first, column structure menu indicates the live date column structure

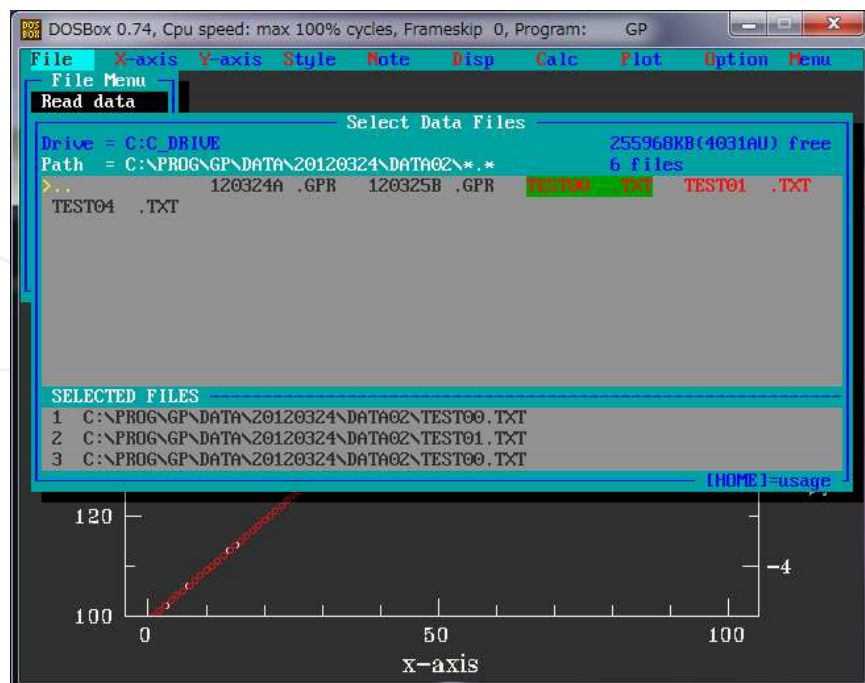


Figure 12. Second, load file name menu indicates the live date formatted general-purpose text-style pursuant to table 3a,3b

x-axis-data	y- axis-data
A main title of presented Graph	
A title of x-axis	
A title of y-axis	
1.022326732	100
2.010754735	101
2.943458995	102
4.094871558	103
4.993183668	104
6.073690076	105
7.054419829	106
•	•
•	•
•	•
97.94832211	197
98.91335378	198
100.0896175	199

a

x-axis-data	y- axis-data
A main title of presented Graph	
A title of x-axis	
A title of y-axis	
1.00	100
2.00	101
3.00	102
4.00	103
5.00	104
6.00	105
7.00	106
•	•
•	•
•	•
98.00	197
99.00	198
100.00	199

b

Table 3. a. Typical numerical example for differential calculation with random number generator only inside x-axis formatted for GP.exe as data filename TEST01.TXT b. Typical numerical example for differential calculation formatted for GP.exe as data filename TEST00.TXT



Figure 13. Third, load parameter's file menu indicates organized graph structure

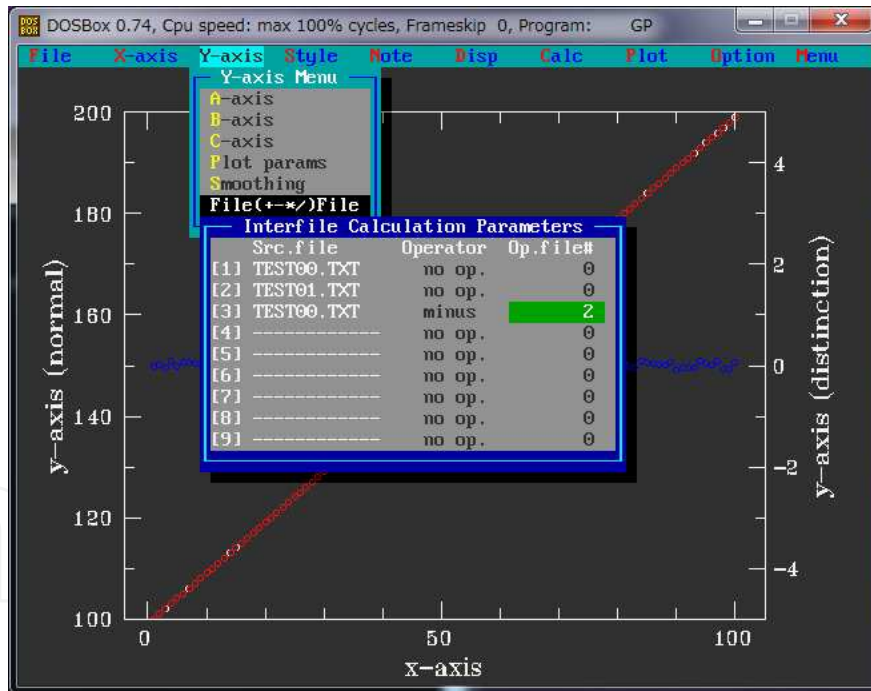


Figure 14. Forth, an Interfile Calculation Parameters and style-menu displayed, red-mark of TEST01 (Src. file # 2) on left-y-axis and white-mark of TEST00 (Src. file # 1) on left-y-axis, meanwhile blue-mark of TEST00 minus TEST01 (Src. file #3 minus #2) on right-y-axis. In the figure, a highlight area of green, the letter of the 2 means the #2 file that selected for Src. file #3 minus #2.

In the Fig. 15., Left and right axis, so called Y-axis Plotting Parameters are shown relation to Fig.14. For Src. file #1 and 2 are to belong to left-y-axis named A of Y-axis and further calculated Src. file #3 minus #2 is to belong to right-y-axis named B.

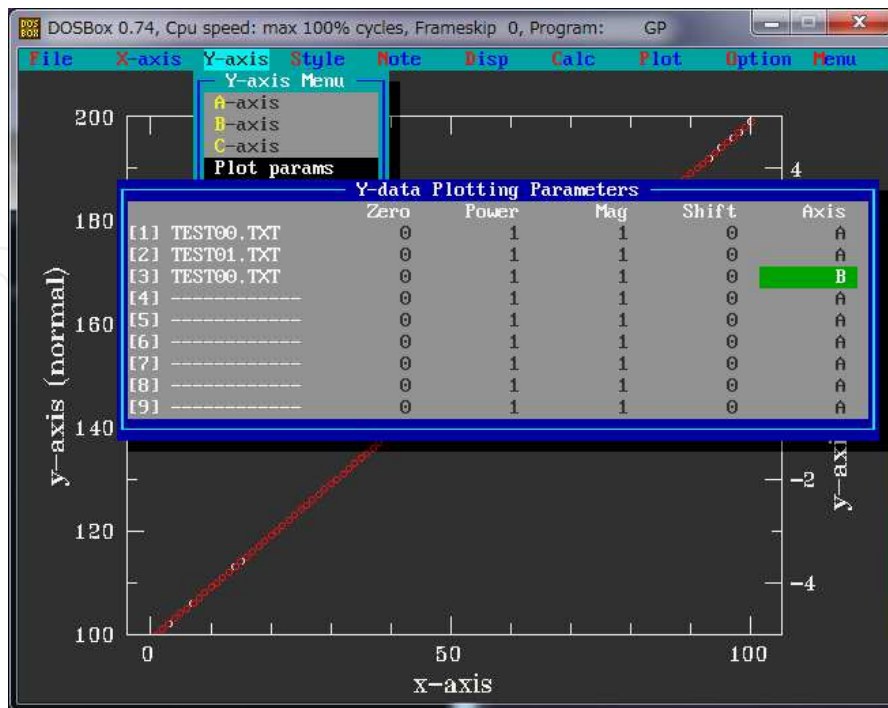


Figure 15. Fifth, Y-axis Plotting Parameters are shown. For Src. file #1 and 2 are to belong to left-y-axis named A and Src. file #3 minus #2 (calculated data) is to belong to right-y-axis named B

In the Fig. 16., Plotting green cross-line indicator means the calculated Src. file #3 minus #2 dots. Fig. 10s are also the similar for usage of cross-line indicator.

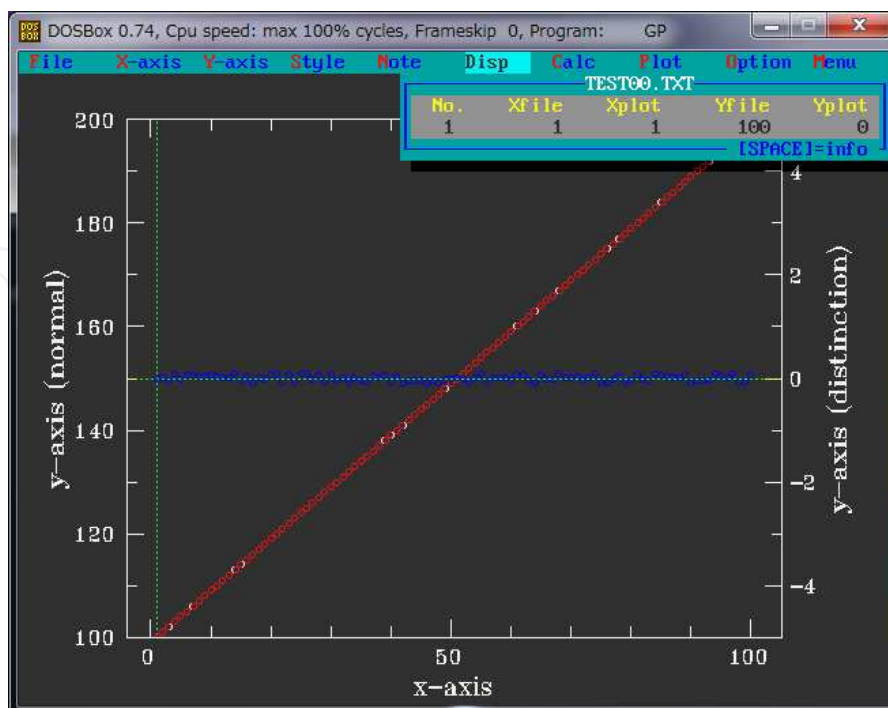


Figure 16. Sixth, Plotting green cross-line indicator means the calculated Src. file #3 minus #2 dots

In the Fig. 17., It is the most important method for calculating of relaxation process. Text-fire save-menu using blue-mark of TEST00 minus TEST01 (Src. file #3 minus #2) on right-y-axis should be describe for example as file name TEST04.TXT in write-data filename input region. Then the TEST04.TXT should be on further calculation process to equation (5) , $t=1(s)$, then should be normalized and multiplied by inverse reactor summation.

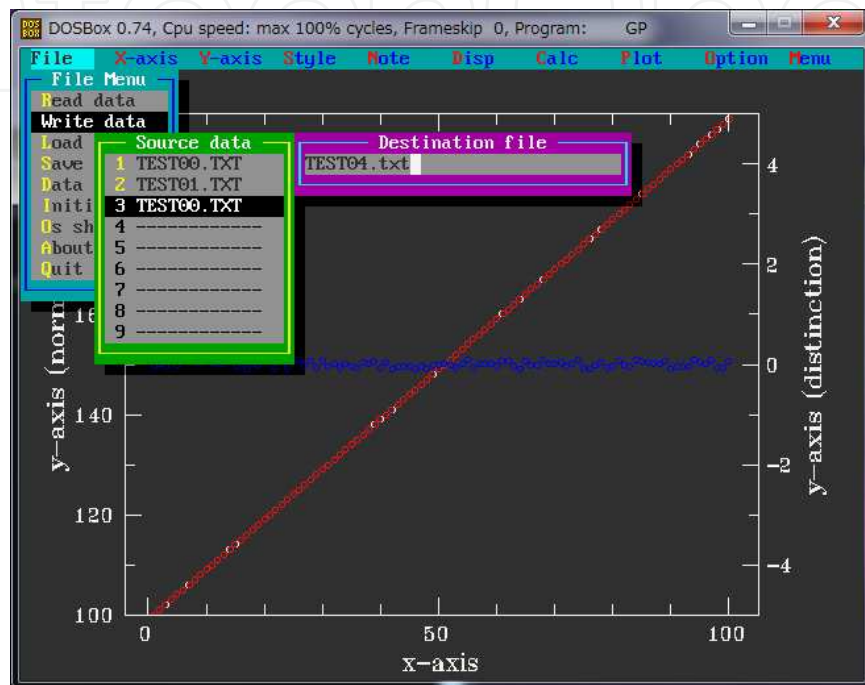


Figure 17. Seventh, text-fire save-menu using blue-mark of TEST00 minus TEST01 (Src. file #3 minus #2) on right-y-axis as file name TEST04.TXT displayed in write-data panel

In the Fig. 18., PostScript-file save-menu using a PostScript-file driver of PS.DLL, that include gpat431.lzh archive, displayed in Plot Parameters panel. Furthermore the useful information, if it assumed to be a 01.ps as saved file name for presented graph design, it would be transformed from PostScript-file to PDF-file, for example, from 01.ps to assumed 01gw.pdf, to be free to use a program ghostscript ver. 9.04. It should be typed on command-line supported by each OS in current directory of 01.ps (not use the command-line in DOSBox) as:

```
"C:\Program Files\gs\gs9.04\bin\gswin32c.exe" -dNOPAUSE -dBATCH -sDEVICE = pdfwrite -r600 -sOutputFile = 01gw.pdf -c 300000 setvmthreshold save pop -f 01.ps
```

Assumed 01gw.pdf would be a graph with super-resolution quality attaching suitable for all kind of publications. For example, it could be transformed from their PDF to word-processor MS-Word, to be free to use a program such as "Acrobat Reader", and it should be typing keys of Control-a, then Zoom up to around 200%, then Control-c, after then in word-processor to be also typing keys Control-v for universal use.

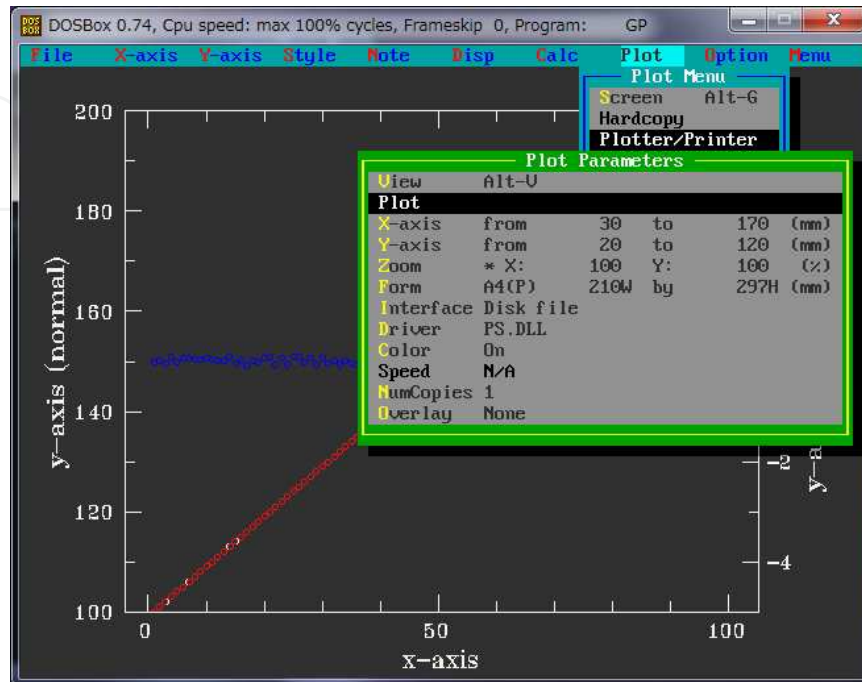


Figure 18. Final, PostScript-file save-menu using a PS.DLL PostScript-file driver displayed in Plot Parameters panel. If it assumed to be a 01.ps as saved file name, it would be transformed from PostScript-file to PDF-file, for example, from 01.ps to assumed 01gw.pdf, to be free to use a program ghostscript ver. 9.04. It should be typed on command-line as:
`"C:\Program Files\gs\gs9.04\bin\gswin32c.exe" -dNOPAUSE -dBATCH -sDEVICE=pdfwrite -r600 -sOutputFile=01gw.pdf -c 300000 setvmthreshold save pop -f 01.ps`

5. Conclusion

In the present work for calculation using specific normalized 1st derivative - type relaxation ratio function of $\theta(E, T, t=1s)$, activation energy spectrum distributed in $\text{Cu}_{60}\text{Hf}_{20}\text{Ti}_{20}$, $(\text{Cu}_{60}\text{Hf}_{22}\text{Ti}_{18})_{0.99}\text{B}_1$ and $(\text{Cu}_{60}\text{Hf}_{22}\text{Ti}_{18})_{0.97}\text{B}_3$ have been observed through the process of numerical-based discussion. It is so called rapid-type clarification between the temperature range T_2 and T_1 for almost around narrow 100 K region. In other words, even the above mentioned narrow temperature range induced the "reversible" phenomena, and it has been also observed in the anneal process of scan #1 to #n, repeatedly.

After it has been difficult in general to calculate numerical differences between any kinds of DSC live data. Because it has the time-domain problem for stepping accuracy and speed on temperature column region. So in second half of this paper, it was tutorial to short course calculation method for the differences using the freeware in Tohoku University Prof. K.

Edamatsu' GP.EXE that was designed until 1999 to make smart graphs for publication with powerful data analysis ability such as numerical complex differentiation. And now it is shown that the GP.EXE has been useful for genuine data processing even in the 2012's generation.

Author details

Kazu-masa Yamada
*Hakodate National College of Technology,
 Department of Electrical and Electronic Engineering,
 Japan*

Acknowledgement

The author was favoured to have the assistance of Dr. I. A. Figueroa in Universidad Nacional Autonoma de Mexico who contributed an experimental circumstance to the accomplishment of the amorphous sample preparations in the University of Sheffield UK. The author also would like to express the appreciation to Dr. Sergio Gonzalez Sanchez (Universitat Autonoma de Barcelona), Mr. P. J. J. Hawksworth and Dr. I. Todd in the University of Sheffield. The author is indebted to Professor H. A. Davies for drawing his attention to presented researches.

6. References

- [1] Brochure for the Nanotechnology and Materials Technology Development Department, on March (2008), The New Energy and Industrial Technology Development Organization (NEDO) in Japan, processing technology for metallic glasses, p.61-62, http://www.nedo.go.jp/kankobutsu/pamphlets/nano/nano_e2008.pdf
- [2] I.A. Figueroa, R. Rawal, P. Stewart, P.A. Carroll, H.A. Davies, H. Jones and I. Todd, *Journal of Non-Crystalline Solids*, Vol. 353 (2007), pp. 839-841
- [3] I.A. Figueroa, H.A. Davies, I. Todd and K. Yamada, *Advanced Engineering Materials*, Vol. 9 (2007), pp. 496-499
- [4] K. Yamada, Y. Iijima and K. Fukamichi: *Defect and Diffusion Forum*, Vols. 143-147 (1997), pp.765-770
- [5] K. Yamada, Y. Iijima and K. Fukamichi: *J. Mater. Res.*, Vol. 8 (1993), pp.2231-2238
- [6] Y. Takahara, A. Morita, T. Takeda and H. Matsuda: *J. Japan Inst. Metals*, Vol. 54 (1990) pp. 752-757 (in Japanese)
- [7] K. Yamada, M. Ito, M. Tatsumiya, Y. Iijima and K. Fukamichi: *Defect and Diffusion Forum*, Vols. 194-199 (2001), pp.815-820
- [8] K. Yamada, K. Fukamichi and Y. Iijima: *J. Magn. Soc. Jpn.*, Vol.22 Suppl. S2 (1998), pp. 97-100
- [9] K. Yamada et al, *Defect and Diffusion Forum* Vols. 283-286 (2009), pp 533-538

[10] J. A. Leake, E. Woldt, and J. E. Evetts, *Mater. Sci. Eng.*, Vol. 97 (1988), pp. 469-472

[11] M. R. J. Gibbs, J. E. Evetts and J. A. Leake, *J. Mater. Sci.*, Vol. 18 (1983), pp. 278-288

[12] W. Primak: *Phys. Rev.* Vol. 100 (1955) pp. 1677-1689

IntechOpen

IntechOpen